INTERNATIONAL JOURNAL OF HYDROGEN ENERGY 48 (2023) 22277–22287

Available online at www.sciencedirect.com

ScienceDirect

journal homepage: www.elsevier.com/locate/he

Comprehensive analysis on the effect of lube oil on particle emissions through gas exhaust measurement and chemical characterization of condensed exhaust from a DI SI engine fueled with hydrogen

Barbara Apicella, Francesco Catapano, Silvana Di Iorio, Agnese Magno, Carmela Russo, Paolo Sementa, Fernando Stanzione, Antonio Tregrossi, Bianca Maria Vaglieco*

Institute of Science and Technology for Sustainable Energy and Mobility (STEMS) - CNR, Napoli, Italy

HIGHLIGHTS

- Engine performance and pollutant emissions were measured for a DI SI engine fueled with hydrogen.
- Effect of lube oil on particle number and size at exhaust of a hydrogen fueled engine.
- Presence of PAH, alkyl-PAHs, oxy-PAHs and mineral oil in the exhausts.
- A part of the lubricating oil passed into the combustion chamber and underwent thermal degradation.
- Emitted oil presented a good affinity with water thus evidencing its impact also on the water and soil pollution.

GRAPHICAL ABSTRACT

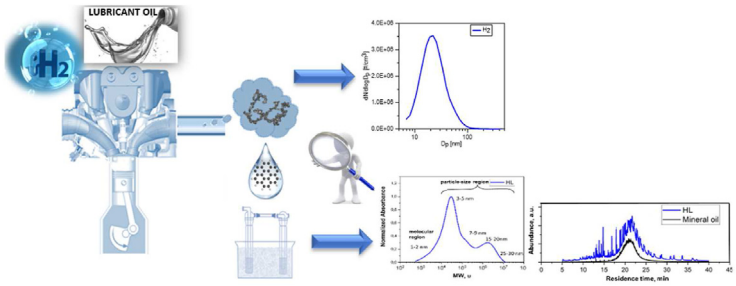

ARTICLE INFO

Article history:
Received 29 November 2022
Received in revised form
13 February 2023
Accepted 9 March 2023
Available online 28 March 2023

ABSTRACT

This research study aims to investigate the causes of the particles emitted by a spark ignition engine fueled with hydrogen. The experiments were carried out on a single cylinder 250 cm^3 direct injection spark ignition engine. Two operating conditions at 2000 rpm both full and low load, representative of typical urban conditions, were investigated. A physical characterization of the particles, size and number, was performed through an Engine Exhaust Particle Sizer coupled to a single diluter. Chemical characterization was carried out on the condensed exhaust. The simultaneous analysis of the physical

* *Corresponding author*. STEMS-CNR, Via G. Marconi 4, 80125, Naples, Italy.
E-mail address: silvana.diiorio@stems.cnr.it (S. Di Iorio).

https://doi.org/10.1016/j.ijhydene.2023.03.112

Keywords:
Hydrogen
Particle emission
Lube oil
PAH
Particulate matter

properties and their chemical characterization allows to point out not only the role of the oil on the particle emissions but also to give an important information on its state/composition, if it was unburned and oxidized. Particles were detected with conventional spectrometer at low load while at high load the noise signal ratio is too high to distinguish the presence of particles. More detailed chemical techniques highlighted the presence of PAH, alkyl-PAHs, oxy-PAHs and unburned hydrocarbon in the exhaust due to the mineral oil.

Introduction

The melting of glaciers and the consequent rising of the sea level as well as the increasing of epidemic diseases are becoming even more frequent and can be ascribed to the rise in temperature. The main cause of the climate changes is the larger presence of greenhouse gases due to increased industrialization and energy demand [1].

In the urban area, the most important factor responsible of the deterioration of the local air quality is the transportation which currently is mainly entrusted to the internal combustion engines (ICEs) powered by fossil fuels. Despite the great efforts paid to improve the combustion as well as to develop more efficient after-treatment systems, ICE still remains a significant source of pollutants.

The battery electric vehicles (BEVs) are considered a promising way to make the transport sector more environmentally friendly. Anyway, the BEVs do not represent a short-term solution since a large investment in charging infrastructure and electricity generation is needed before a widespread adoption of BEVs occurs. It is reasonable that in this transition period the ICEs will still be the main driven power of transport, particularly for the commercial one [2,3].

Considering that the formation of carbon dioxide (CO_2) and particles is due to the carbon atoms in the fuels [4], fuel decarbonization has been promoted [5,6] to face the climate changes. Thus, zero/low carbon fuels, such as methane, hydrogen, methanol, are playing an even more attractive role.

Gaseous fuels such as Compressed Natural Gas (CNG) and hydrogen are very attractive alternative fuels [7] because of their low environmental impact and wide reserves localizations [8–10]. They can be used both alone and dual fueled [11–13].

In the past years, great attention was paid to the CNG because of its large availability, its low prize and the better CO_2 footprint compared to conventional fuels because of its lower carbon content [14]. Moreover, it allows to reduce also the emissions of particles, carbon monoxide (CO) and nitrogen oxides (NO_x) with respect to gasoline and diesel fueled engines. On the other hand, CNG is characterized by a slow flame propagation speed and poor lean-burn capability resulting in lower efficiency and higher instability [15,16].

Hydrogen has also attracted a lot of attention because it is a zero-carbon fuel. Another aspect to consider is that hydrogen can be obtained by renewable alternative fuels, which can be produced through electrolysis of water, gasification of coal, biomass and steam reformation of natural gas [17]. Hydrogen is a promising fuel for the spark ignition (SI) engines due to its properties such as the higher RON, the higher flame propagation speed, the higher calorific value and the lower ignition energy. Moreover, it allows working in lean conditions guaranteeing a stable combustion [18].

Several studies highlighted the improved combustion, engine performance and emission reduction due to hydrogen [19]. Theoretically, its combustion produces only water vapors and NO_x. Anyway, hydrogen fueled engines emit also particles [20].

Typically, the main source of particulate matter in ICEs is the fuel even if several studies evidenced that the contribution of lubricating oil on its emissions is not negligible [21,22].

If the fuel is hydrogen, as it has no carbon atoms in its molecule, just the lubricating oil is responsible of the particle formation. Singh et al. [23] performed a comparison between diesel, gasoline, CNG, HCNG and hydrogen. Their study pointed out that the role of oil on particle formation is more predominant for hydrogen fueled engine. Miller et al. [24] reported that the lubricating oil from a hydrogen powered engine do not burn completely forming unburned hydrocarbons and polycyclic aromatic hydrocarbons (PAHs) and consequently particles. In another study, Singh et al. [25] explored the differences between the particle characteristics of a hydrogen fueled engine when ignited with laser induced system and a conventional spark plug, highlighting the effect of ignition mode on the oil pyrolysis. Thawko et al. [26] performed a comprehensive analysis on the particle emissions from direct injection (DI) engine fed with a hydrogen-rich reformate. They observed that the total particle number concentration strongly depends on the fuel type and fuel injection strategy.

Another aspect beyond the impact of the particles on atmospheric emissions is the impact of the condensed exhaust on the soil pollution. A large amount of PAHs, known to be mutagen and carcinogen [27], in fact, is found in the soil and the vehicle emissions are the principal source of these PAHs in the roadside soils [28,29].

Several studies evidenced the presence of particles at the exhaust of hydrogen-fueled engine. However, the role of the lubricating oil on the mechanisms of particle formation is still not clear.

In this framework, this study aims to investigate the role of lubricating oil on the particle emissions. The experimental investigation was performed on a small displacement DI SI engine. The engine run at 2000 rpm both at full and low load. These operating conditions correspond to different level of lubricating oil in the combustion chamber. An Engine Exhaust

Particle Spectrometer (EEPS) from TSI coupled to a single diluter (SD) was used for the sizing and counting of the particle. The chemical characterization was performed on the condensed exhaust and particles by using a condensation sampling line connected to the tailpipe. The condensed exhaust and particles were collected in cooled traps and filters and off-line analyzed with a plethora of analytical techniques.

Experimental apparatus and methods

Test engine

The experimental facilities include the test engine loaded by an electrical dynamometer to manage the load and speed and the data acquisition system. The engine is a water-cooled, single cylinder, SI, operating on a four-stroke cycle whose main characteristics are listed in Table 1. It is equipped with a prototype cylinder head with a DI system. The engine head has four valves pent-roof shaped combustion chamber with a spark plug flush-mounted in the center.

A commercial lubricant oil obtained by a combination of synthetic and mineral bases with 10W–40 viscosity grade was used. Table 2 shows the mail lubricant oil properties.

Hydrogen is directly injected in the combustion chamber by an air assisted Synerject strata injector [30]. It was installed inside the cylinder between the intake valves to ensure hydrogen injection. Hydrogen was provided by a compressed bottle at 200 bar and decompressed to 6.5 bar through a regulator and, then, injected into the cylinder. To ensure safety operating conditions, a flame arrestor and a pneumatic-actuated valve installed downstream of the pressure regulator allow to provide the gaseous fuel to the injector only in running mode.

Table 1 – Engine specifications.

Engine	Spark Ignition
Number of Cylinders	1
Bore [mm]	72
Stroke [mm]	60
Displacement [cm^3]	244.3
Compression Ratio	11.5:1
Max. Power [kW]	16 @ 8000 rpm
Max. Torque [Nm]	20 @ 5500 rpm
Intake	Naturally Aspirated
Injection system	DI Prototype

Table 2 – Lubricant oil properties.

Properties	
Viscosity	10W-40
Density @ 20 °C	0.870 kg/l
Viscosity @ 40 °C	101.7 mm^2/s
Viscosity @ 100 °C	14.5 mm^2/s
Viscosity index	151
Pour point	−35.0 °C
TBN	10.1 mg KOH/g
Flash point	228 °C

Table 3 – AVL Digas 4000 specifications.

	Measurement range	Resolution
CO	0–10% vol.	0.01% vol.
CO_2	0–20% vol.	0.1% vol.
HC	0–20,000 ppm vol.	1 ppm
NO_x	0–5000 ppm vol.	1 ppm
O_2	0–25% vol.	0.01% vol.

K-type thermocouples were used to monitor the temperature at both inlet and exhaust as well as the oil and coolant temperatures. A linear lambda sensor Bosch LSU 4.9 was mounted in the exhaust manifold to measure the excess air ratio (λ) value. A crank-shaft encoder AVL 365 was used for engine crank angle detection. In-cylinder pressure was monitored through an AVL GH12D piezoelectric pressure transducer flush-mounted in the area between the intake and exhaust valves. The charge output from this transducer was converted to an amplified voltage using the AVL FlexIFEM Piezo charge amplifier.

The operating system consists on an AVL Engine Timing Unit (ETU) multi-channel system allowing flexible control of injection and ignition timing.

The high-speed data acquisition system AVL IndiModul recorded the signals from all the sensors mounted on the engine. Real time combustion analysis was carried out by the AVL IndiCom software. Pressure signals of 200 cycles were recorded and they were post-processed for thermodynamic analysis.

Gaseous emission measurement

The gas emission analyzer AVL Digas 4000 (Table 3) measured the regulated exhaust emissions that are NO_x, hydrocarbons (HC), CO and CO_2.

Particle measurement system, condensed exhaust sampling procedure and sample treatment

Particle number and size characterization was carried out with high accuracy and reproducibility by means of the EEPS 3090 from TSI [31] whose main characteristics are listed in Table 4. The instrument allows to measure the particles in the size range from 5.6 to 560 nm without discriminating their nature, if solid or volatile, at the rate of 10 Hz. The measurement principle in based on the electrical mobility diameter. Particles entering the measurement region are charged by applying an electric field and the current produced by the electrometers

Table 4 – EEPS specifications.

Particle Size Range	5.6–560 nm
Particle Size Resolution	16 channels per decade (32 total)
Electrometer Channels	22
Charger Mode of Operation	Unipolar diffusion charger
Inlet Cyclone 50% Cutpoint	1 μm
Time resolution	10 size distributions/sec
Inlet Aerosol Temperature	10–52 °C

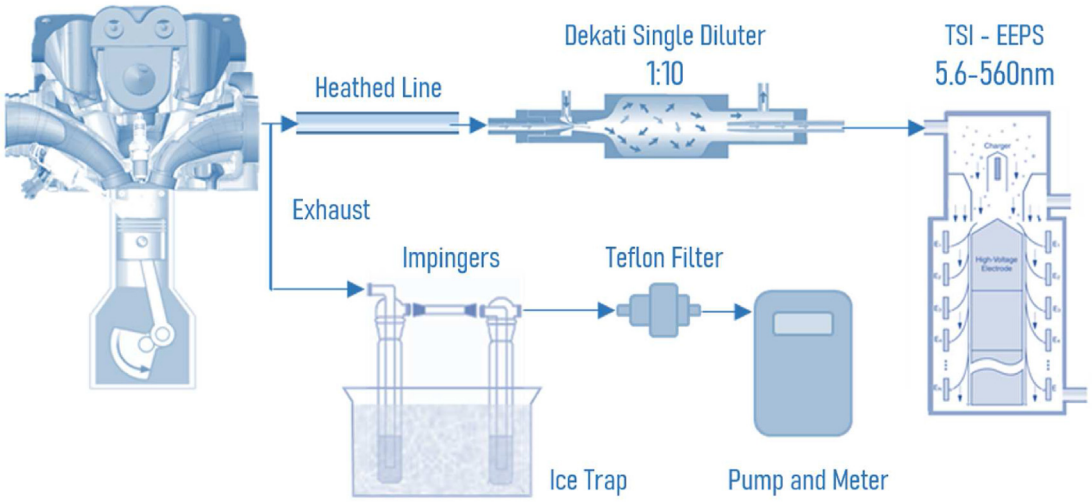

Fig. 1 – Experimental setup for particle measurement and for condensed exhaust sampling.

where the particles impact on is detected and converted in particle concentration through an inversion algorithm [32].

The sampling occurs through a heated line set at 150 °C and a single stage hot dilution, 150 °C.

A sketch of the sampling line is reported in Fig. 1. More details on the sampling systems and on the sample treatment to recover the soluble organic fraction (SOF) in dichloromethane (DCM) from both combustion water and sampling line are reported in Ref. [33]. The volume of the SOF solution in DCM was firstly reduced to 1 ml to perform spectroscopic measurements and then to 0.1 ml for gas chromatography mass spectrometry (GC-MS) analysis.

GC-MS and spectroscopic analysis were performed also on the lubricant oil utilized in the engine for comparison.

Both SOF and particles, if present, were diluted in N-methyl pyrrolidone (NMP) for size exclusion chromatography analysis.

Analytical techniques: chemical and spectroscopic techniques

Chemical and spectroscopic techniques were applied to characterize the condensed exhaust. For the sampling of condensed exhaust, the engine run at fixed operating condition for about 1 h. Three sampling at different days were realized. The total uncertainty of the chemical and spectroscopic results due to both the sampling and analytical procedure was about 15%.

The GC-MS employed is an AGILENT GC 6890 - MSD 5975C. The mass spectrometer operated in electron ionization mode, and *m/z* was scanned from 50 to 400. PAH concentrations were determined using response factors from standards species. More details on GC-MS analysis are reported in a previous work [34].

Table 6 – Combustion parameters.

	λ [–]	IMEP [bar]	COV IMEP [–]
LL	1.6	4.1	0.9
HL	1.5	5.5	1.2

UV–Visible and fluorescence spectra of combustion water and of SOF samples dissolved in DCM, were measured on an HP 8453 Diode Array spectrophotometer and a HORIBA Scientific FluoroMax-Plus TCSPC spectrofluorometer, respectively, using 1 cm quartz cuvettes. More details on the acquisition of fluorescence spectra are reported in Ref. [35].

Molecular weight (MW) distribution of condensed exhaust samples were measured by size exclusion chromatography (SEC) by elution with N-Methyl-2-pyrrolidonen (NMP) on a HPLC system HP1050 series equipped with an UV–Visible diode array detector fixed at 350 nm. Two different columns were used: a highly cross-linked "individual-pore" column (Polymer Laboratories, Ltd., U.K.; particle size of 5 μm diameter and a pore dimension of 50 nm) and a Jordi Gel DVB Column for mass determination in the 100 – 2E4 u range (corresponding to sizes up to about 3–4 nm) and in the 2E3-4E9u range, respectively. The Sample MW was determined by calculating the retention time on the SEC columns of polystyrenes standards species. More details on SEC apparatus are reported in Ref. [36].

Operating conditions

Experiments were carried out in steady state conditions after proper engine warming up. Tests were carried out at engine speed of 2000 rpm, at both low (LL) and high load (HL). The

Table 5 – Operating condition.

	Engine speed [rpm]	Throttle opening [%]	DOI [cad]	SOI [cad]	SOS [cad]	λ [–]	Texhaust [°C]
LL	2000	15	170	−270	7.0	1.6	360
HL	2000	95	225	−260	11.6	1.5	390

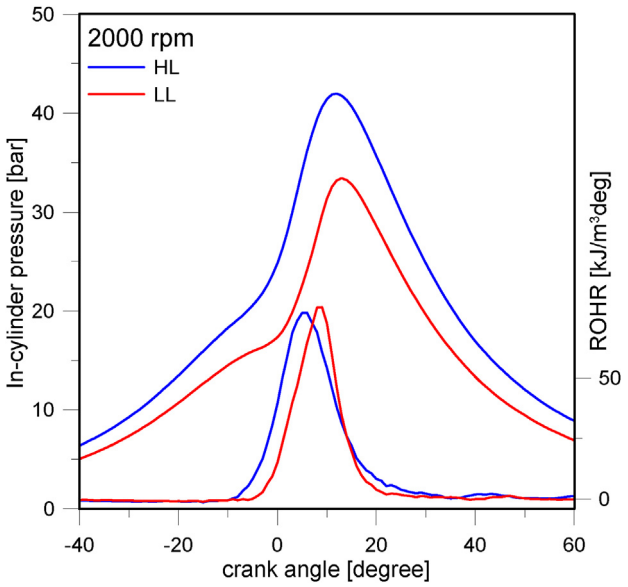

Fig. 2 – In-cylinder pressure and the ROHR measured at 2000 rpm in LL and HL conditions.

engine was operated in lean condition to improve performance and reduce the NO_x emissions. Table 6 shows the investigated test conditions. The start of injection (SOI) and start of spark (SOS) were properly set to guarantee a stable combustion. Duration of injection (DOI) was varied according to the desired load and air-to-fuel ratio. Table 5.

Experimental results

The experimental study was divided in two parts. The first part was devoted to the analysis of the combustion process and the characterization of the gaseous and particle emissions. In the second part a chemical analysis was carried out on condensed exhaust for a deeper insight on the nature and structure of the particles.

Table 7 – Concentration of NO_x gaseous emissions.

	NO_x [ppm]
LL	1226
HL	1472

Combustion analysis and emission characterization

Indicated data allowed to characterize the combustion process. The in-cylinder pressure was measured over 200 cycles. The rate of heat release rate (ROHR) normalized with cylinder volume was calculated from the pressure data. The indicated mean effective pressure (IMEP) gives information on engine performance and the coefficient of variance (COV) of the IMEP allows to evaluate the combustion stability. The in-cylinder pressure and the ROHR are depicted in Fig. 2 for LL and HL conditions.

The in-cylinder pressure is higher at high load because of the larger injection of fuel to meet the higher power demand. The ROHR shows the same behavior despite the load conditions. Only the premixed combustion mode is distinguishable from the ROHR curves. The main combustion parameters are listed in Table 6.

The IMEP is higher at HL condition because of the larger fuel and then energy supply. There are no differences in terms of the stability of the combustion, the COV of IMEP is, in fact, about 1 at both operating conditions.

As hydrogen does not contain carbon, carbon emissions, such as CO, HC, and CO_2, were not produced, only NO_x was measured at the exhaust. The concentrations of the NO_x emissions measured at both LL and HL conditions are listed in Table 7.

The NO_x emissions are higher at HL condition because of the higher in-cylinder temperature. The temperature and λ influence the NO_x emissions. The higher the temperature, the larger NO_x emissions. Regarding the dependence with air excess, NO_x increases with the λ until the stoichiometric value then starts to decrease. In this case, operating at lean condition, the driven mechanism is the temperature.

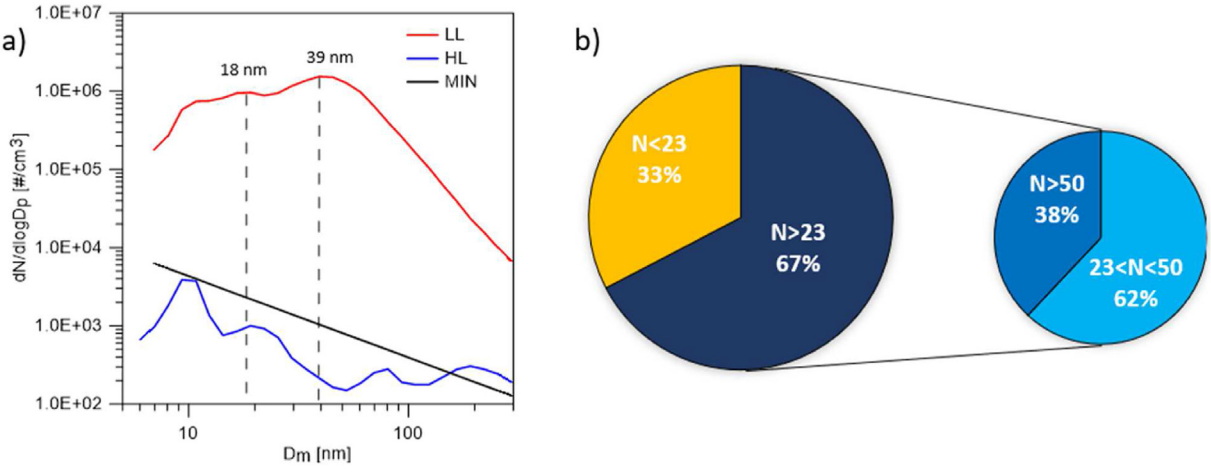

Fig. 3 – a) PSDs at LL, HL and MIN and b) number concentration at different size classes at 2000 LL.

The particle emissions strongly depend on the engine operating condition. At HL the Signal Noise Ratio is too low, the particle size distribution (PSD) is in fact within the limit values, MIN, corresponding to the electrical noise of the instrument so it is not possible to have relevant information. On the other hand, at LL a significant number of particles was measured, as evidenced in Fig. 3 where the PSDs measured at 2000 rpm HL and LL and the number concentration at different size classes at LL are depicted.

The formation of particles cannot be ascribed to the fuel but rather to the incomplete combustion of the lubricating oil present in the combustion chamber. Particles show a well-defined bimodal size distribution. The first peak is centered around 18 nm and the second and higher peak around of 39 nm. The differences observed between the LL and HL conditions can be ascribed to the different environmental condition and level of oil in the combustion chamber. In LL condition due to depression downstream of the throttle, more oil vapors enter in the combustion chamber thus taking part to the combustion and contributing to the particle emissions. Moreover, due to the lower temperature typical of this condition, the piston and rings are not subject to a great deformation so more oil leaks in the combustion chamber can occur. On the other hand, at high load, the piston and ring undergo an expansion that guarantees a better seal because of the higher temperature. It is worth noting that the major contribution to the emissions is due to the particles in the size range from 23 to 50 nm.

Chemical characterization

For a comprehensive understanding of the nature of the particles emitted form hydrogen fueled engines the condensed exhaust was sampled and analyzed with an array of chemical and spectroscopic techniques. The sampling was carried out with the system sketched in Fig. 1.

The condensed water collected in the traps was preliminarily analyzed by fluorescence spectroscopy, before the extraction treatment, and it presented an intense fluorescence emission in a wavelength range typical of aromatic species [37,38]. Whatever the operating conditions, the results evidenced the presence of similar species but with different concentrations. The combustion water was then extracted by DCM and the extraction process required at least three extraction steps, demonstrating the high affinity of the exhaust oil with water, which is of concern for its environmental impact. For obtaining a comparison with the online measurements, preliminarily the MW distribution of SOF at HL and LL conditions was evaluated, drying the samples in DCM and dissolving them in NMP for SEC analysis with two different columns (see session 2.4 for details). In Figs. 4 and 5 the MW distributions obtained with non-porous column (larger MW range) and not-mixed column (smaller MW range) are reported, respectively. It is possible to observe in Fig. 4 that the distribution is peaked at MW corresponding, on the basis of polystyrenes and PAHs calibration [39], to a MW consistent with a dimension of 3–4 nm (assuming spherical shape and a density in a range between 1.2 and 1.8 kg/l [40]) both for LL and for HL samples with a tail at a larger MW, corresponding to 15–20 nm for HL and 25–30 nm

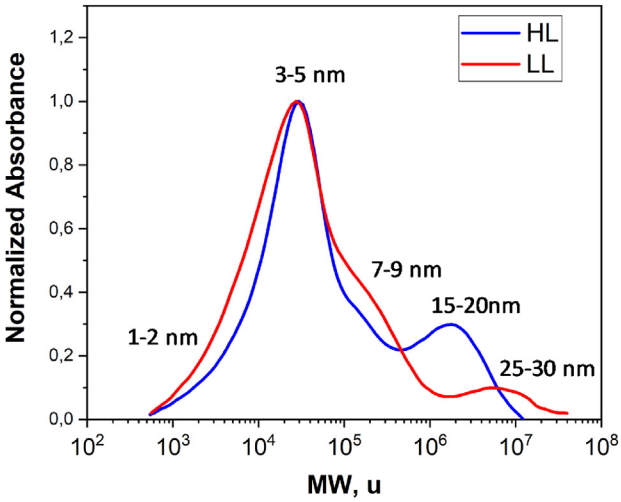

Fig. 4 – MW distribution profiles of the SOF samples from SEC with non-porous column of HL and LL samples, acquired with UV–Visible detector at 370 nm.

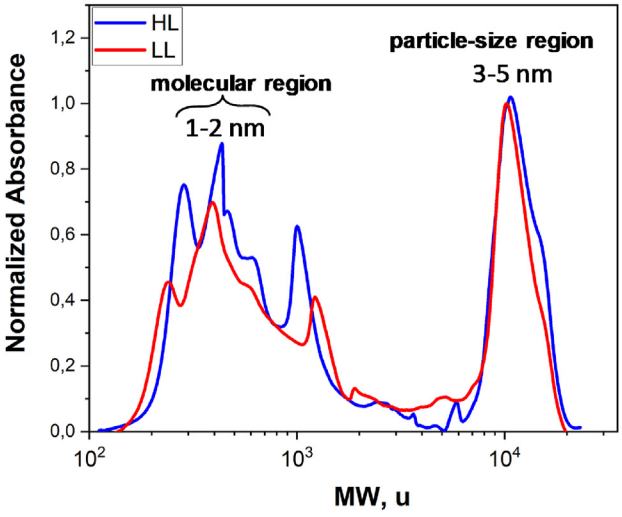

Fig. 5 – MW distribution profiles of the SOF samples from SEC with not mixed column of HL and LL samples, acquired with UV–Visible detector at 370 nm.

for LL. Looking also to the molecular region (Fig. 5), both the exhaust samples present again very similar distributions in the range around 1–2 nm.

The MW, Fig. 4, and the PSD, Fig. 3, offers complementary information. The first allows off-line measure of MW corresponding to particles from 1 up to 30 nm, the second to detect on-line the particles size from 6 to 560 nm. Moreover, the two techniques are characterized by a different sensibility giving the possibility to detect particles also at low and high concentration. A good agreement was observed between MW and the PSD in the common size region at LL, both in fact evidenced a large presence of particles in the size range 7–30 nm. Considering the different basic principle of the two techniques and the different methods of analysis (on-line and off-line), the quite good agreement observed offers a mutual validation of analytical and sampling techniques. Moreover, the SEC

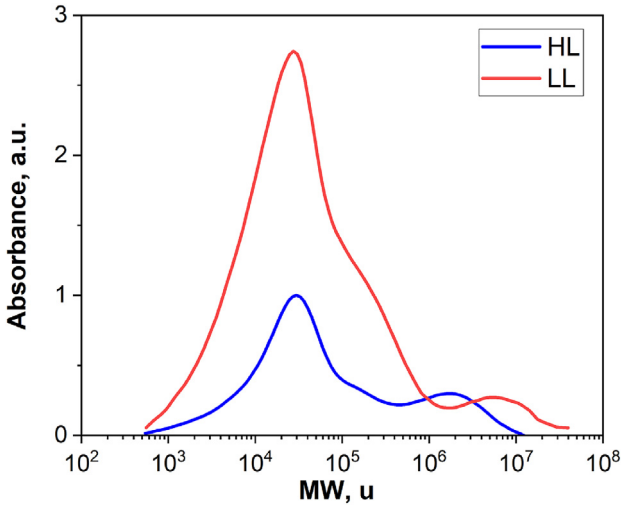

Fig. 6 – MW distribution profiles of the SOF samples from SEC with non-porous column of HL and LL samples, normalized for the sampling time, acquired with UV–Visible detector at 370 nm.

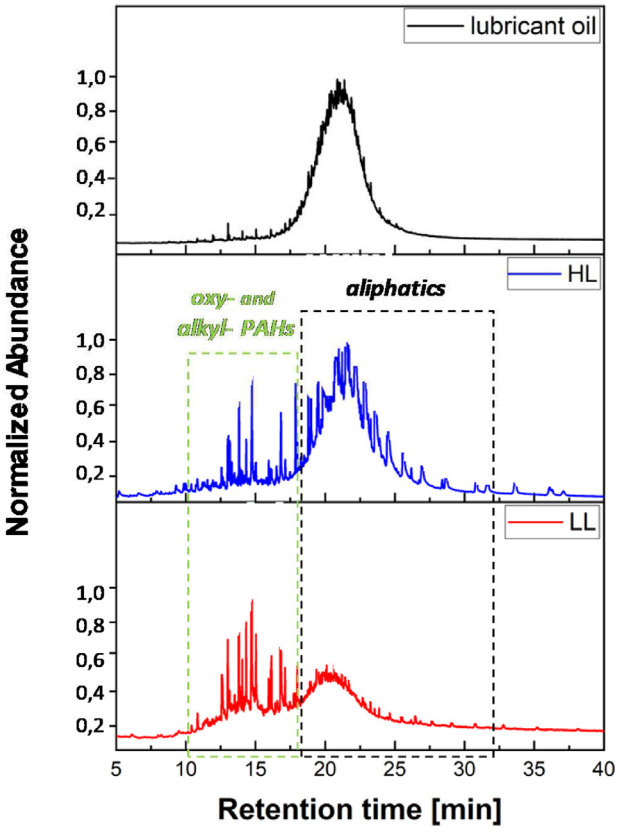

Fig. 7 – GC-MS chromatograms of SOF of HL and LL, along with the lubricant oil chromatogram.

analysis allows also detecting the presence of the particles at HL, which because of the low concentration are not resolvable with the EEPS.

Indeed, comparing the SEC profiles of LL and HL samples normalized for sampling time (Fig. 6), it is possible to observe the very different signal and, therefore, species concentration in the two conditions.

More than the MW distribution, the chemical and spectroscopic techniques applied on the SOF samples allowed to give deep insight on the species composition and structure. The GC-MS chromatograms obtained on the SOF in HL and LL conditions were reported in Fig. 7. In the same Figure, the chromatogram of the lubricating oil was also reported. The chromatograms presented the following features, typical of a mineral oil.

- they have the same unresolved curve
- in both cases a sequence of alkanes was detected by ion extraction.

The observed features can be explained with a leakage of the mineral oil in the combustion chamber, which reached the

Table 8 – Classes of species and major species detected in HL (left side) and LL (right side) SOF by GC-MS, along with their percent mass concentration.

HIGH LOAD		
Classes of species	Species	%
Oxy-PAH	Naphthalenecarboxaldehyde	5–10
	o-Hydroxybiphenyl	
	9H-Fluoren-9-one	
	Anthrone	
	1H-Indene, 2-phenyl-	
Alkyl-PAHs	9H-Fluorene, 2-methyl-	
	Phenanthrene, 1-methyl-	
	Anthracene, 1-methyl-	
Alyphatics (C_{17}–C_{30})	Heptadecane (ene)	90–95
	Octadecane (ene)	
	Eicosane (ene)	
	Heneicosane (ene)	
	Docosane (ene)	
	Tricosane (ene)	
	Tetracosane (ene)	
	Pentacosane (ene)	
	Hexacosane (ene)	
	Octacosane (ene)	
LOW LOAD		
Classes of species	Species	%
Oxy-PAHs	Naphthalenecarboxaldehyde	4–8
	o-Hydroxybiphenyl	
	o-Hydroxybiphenyl	
	9H-Fluoren-9-one	
	Anthrone	
Alkyl-PAHs	Not Detected	
Alyphatics (C_{17}–C_{36})	Heptadecane (ene)	92–96
	Octadecane (ene)	
	Eicosane (ene)	
	Heneicosane (ene)	
	Docosane (ene)	
	Tricosane (ene)	
	Tetracosane (ene)	
	Pentacosane (ene)	
	Hexacosane (ene)	
	Octacosane (ene)	

Of note, only about 60–70% of SOF samples have been detected by GC-MS. The remaining part, undetectable by GC-MS, was investigated by spectroscopic techniques.

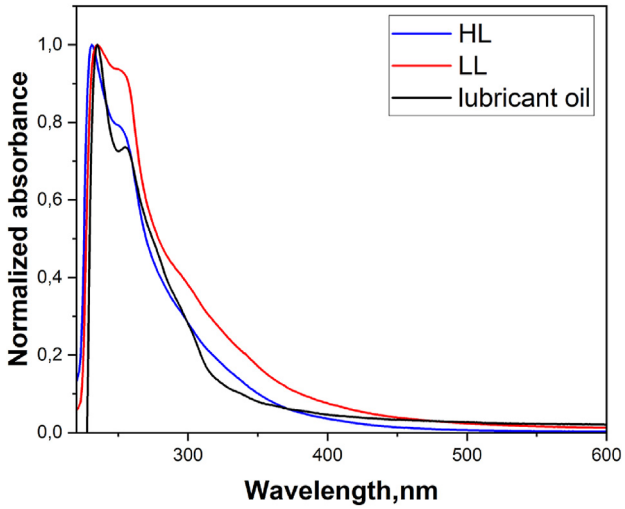

Fig. 8 – Height normalized UV–visible absorption spectra of SOF of HL and LL in DCM, along with the lubricant oil spectrum.

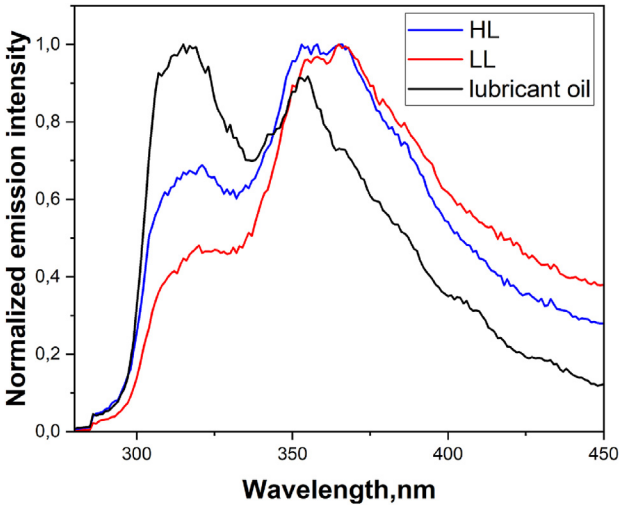

Fig. 9 – Height normalized emission spectra excited at 250 nm of SOF of HL and LL in DCM, along with the lubricant oil spectrum.

exhaust unburned. Moreover, in the SOF samples the presence of alkyl polycyclic aromatic hydrocarbons (alkyl-PAHs) and oxygenated PAHs (oxy-PAHs) were also detected.

The not negligible concentration of these PAHs suggests that a part of the lubricating oil passed into the combustion chamber, both in LL and HL conditions, and was subjected to thermal degradation (oxidation and/or combustion).

The concentration of oil thermal degradation products and residual oil is higher in LL condition. The list of species detected in the two conditions is reported in Table 8. Almost 4–10% of SOF in both conditions is constituted of oxy-PAHs and alkyl-PAHs. The detection of these species is of concern because, although their concentration is very low, they present a toxicity and mutagenicity much high, even higher than that of unsubstituted PAH [41]. Moreover, aliphatics account for 90% of SOF but aliphatic contamination level also showed non-negligible effects on soil bacterial communities to some extents [42].

In Fig. 8, the height normalized UV–visible absorption spectra of HL and LL SOF in DCM, along with the lubricant oil spectrum, are reported. A peak at 250–260 nm is clearly attributable to lubricant. The spectrum after 300 nm, instead, presents broad and higher intensity with respect to lubricant oil, especially in the case of LL SOF. This absorption signal in a region typical of aromatic species, the broadness of the spectrum and the lack of detection by GC-MS allow hypothesizing the presence of high molecular weight aromatic species in SOF samples. They are much more evident in LL SOF, as also observed by the PSD in Fig. 3, where a large number of particles smaller than 23 nm was measured. This hypothesis was confirmed by fluorescence spectra of SOF and lubricant oil, contrasted in Fig. 9, which show an increase of the visible emission for HL and LL SOF with respect to lubricant oil.

This is also more evident in the synchronous fluorescence spectra of oil and SOF reported in Fig. 10. Synchronous fluorescence technique, involving the concurrent scanning of

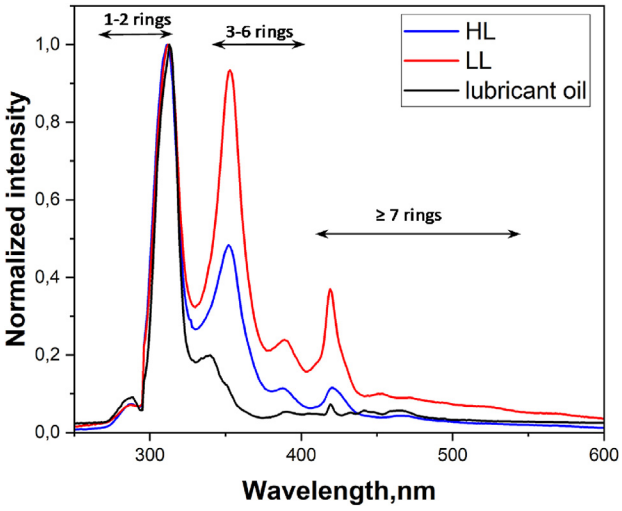

Fig. 10 – Height normalized synchronous fluorescence spectra (Δλ = 10 nm) of SOF of HL and LL in DCM, along with the lubricant oil spectrum.

excitation and emission wavelengths using a Δλ = 10 nm [43], is useful to discriminate between classes of different-sized PAH, thus providing further insights on SOF and oil comparison.

Indeed, consistently with the absorption and emission features (Figs. 8–10), synchronous fluorescence of lubricant oil shows the presence of only mono-ring and two-rings aromatics, whereas HL SOF and, even more, LL SOF synchronous spectra exhibit well-defined peaks due to not only to 1–2 rings but also to 3–6 rings and larger PAH not detectable by GC-MS, typically found in carbon fuels combustion products [38].

These results highlighted the presence of particles and PAHs that are commonly unexpectedly from a hydrogen fueled engine. These pollutants can be ascribed to the

breakdown of the carbon and to the incomplete combustion of organic compounds of lubricating oil.

Conclusions

This study analyzes the effect of lubricating oil on the particle emissions for a hydrogen fueled spark ignition engine by using complementary techniques. Tests were carried out on a small displacement DI SI engine. Engine performance and pollutant emissions were investigated. Pollutants commonly unexpectedly from a hydrogen fueled engine were found. A physical characterization for particle number and size evaluation was performed on diluted exhaust gas. Chemical characterization of both the condensed exhaust and the particle emissions was performed. The main outcomes are following summarized.

- Hydrogen has good potentiality as fuel for spark ignition engine showing a stable combustion in lean conditions even if high NO_x emissions were measured.
- Particles ranging between 10 and 200 nm with two well defined peak at 18 and 39 nm were measured at low load conditions because of the lager presence of oil typical of partial load conditions.
- GC-MS analysis puts in evidence the presence of PAH, alkyl-PAHs, oxy-PAHs and mineral oil in the exhausts. UV–Visible absorption and fluorescence spectroscopy highlights also the contribution of large PAHs not analyzable by GC-MS.
- The presence of high mass aromatic species suggests that a part of the lubricating oil passed into the combustion chamber and degraded at high temperature.

The combination of two different methodologies on both gas and condensed exhaust allowed a comprehensive analysis of the role of lubricating oil on both the particle emissions and high harmful PAHs. Moreover, analytical techniques give relevant information on the mechanisms involved in their formation.

The results demonstrate that hydrogen fueled engine exhaust can contribute to high level of contamination not only of the atmosphere but also of water and soil. Therefore, it is increasingly important to better understand the mechanisms, such as oxidation and dissociation, involved in the oil transformation to properly optimize its formulation.

Credit authorship contribution statement

Barbara Apicella: Methodology, Investigation, Data curation, Writing-original draft, Visualization, Writing-review&editing. **Francesco Catapano**: Methodology, Investigation. **Silvana Di Iorio**: Conceptualization, Methodology, Investigation, Data curation, Writing-original draft, Visualization, Writing-review & editing. **Agnese Magno**: Conceptualization, Methodology, Investigation, Data curation, Writing-original draft, Visualization, Writing-review & editing. **Carmela Russo**: Investigation, Data curation, Writing-review & editing. **Paolo Sementa**: Methodology, Investigation; **Fernando Stanzione**: Investigation. **Antonio Tregrossi**: Methodology, Investigation. **Bianca Maria Vaglieco**: Writing-review & editing, Supervision.

Declaration of competing interest

The authors declare that they have no known competing financial interests or personal relationships that could have appeared to influence the work reported in this paper.

Acknowledgments

Authors thank Carlo Rossi and Bruno Sgammato for the engine assessment and for the support in the experimental activity.

Abbreviations

BEV	Battery Electric Vehicle
CNG	Compressed Natural Gas
CO	Carbon monoxide
CO_2	Carbon dioxide
COV	Coefficient of Variance
DCM	Dichloromethane
DI	Direct Injection
DOI	Duration of Injection
EEPS	Engine Exhaust Particle Spectrometer
ETU	Engine Timing Unit
GC/MS	Gas Chromatography Mass Spectrometry
HC	Hydrocarbons
HL	High load
ICE	Internal Combustion Engine
IMEP	Indicated Mean Effective Pressure
λ	Excess air ratio
LL	Low load
MW	Molecular Weight
NMP	N-methyl pyrrolidone
NO_x	Nitrogen Oxides
PAH	Polycyclic Aromatic Hydrocarbons
PSD	Particle Size Distribution
ROHR	Rate of Heat Release Rate
SD	Single Diluter
SEC	Size Exclusion Chromatography
SI	Spark Ignition
SOF	Soluble Organic Fraction
SOI	Start of Injection
SOS	Start of Spark

REFERENCES

[1] Masson-Delmotte V, Zhai P, Pörtner H-O, Roberts D, Skea J, Shukla P, et al. PPCC, 2018: summary for policymakers. In: Global Warming of 1.5°C. An IPCC Special Report on the impacts of global warming of 1.5°C above pre-industrial levels and related global greenhouse gas emission pathways.

Cambridge, UK and New York, NY, USA: the context of strengthening the global; 2019. https://doi.org/10.1017/9781009157940.
[2] Reitz RD, Ogawa H, Payri R, Fansler T, Kokjohn S, Moriyoshi Y, et al. IJER editorial: the future of the internal combustion engine. Int J Engine Res 2020;21:3–10. https://doi.org/10.1177/1468087419877990.
[3] Kalghatgi G. Is it really the end of internal combustion engines and petroleum in transport? Appl Energy 2018;225:965–74. https://doi.org/10.1016/j.apenergy.2018.05.076.
[4] Haynes BS, Wagner HG. Soot formation. Prog Energy Combust Sci 1981;7:229–73. https://doi.org/10.1016/0360-1285(81)90001-0.
[5] Catapano F, Iorio S Di, Magno A, Sementa P, Vaglieco BM. Effect of ethanol blends , E10 , E25 and E85 on sub-23 nm particle emissions and their volatile fraction at exhaust of a high-performance GDI engine over the WLTC. Fuel 2022;327:125184. https://doi.org/10.1016/j.fuel.2022.125184.
[6] Catapano F, Di Iorio S, Magno A, Vaglieco BM. Effect of fuel quality on combustion evolution and particle emissions from PFI and GDI engines fueled with gasoline, ethanol and blend, with focus on 10–23 nm particles. Energy 2022;239:122198. https://doi.org/10.1016/j.energy.2021.122198.
[7] European Commission. Directive 2014/94/EU - deployment of alternative fuels infrastructure. Off J Eur Union 2014;L307:20.
[8] Zareei J, Rohani A. Optimization and study of performance parameters in an engine fueled with hydrogen. Int J Hydrogen Energy 2020;45:322–36. https://doi.org/10.1016/j.ijhydene.2019.10.250.
[9] Ma F, Liu H, Wang Y, Li Y, Wang J, Zhao S. Combustion and emission characteristics of a port-injection HCNG engine under various ignition timings. Int J Hydrogen Energy 2008;33:816–22. https://doi.org/10.1016/j.ijhydene.2007.09.047.
[10] Thiruvengadam A, Besch M, Padmanaban V, Pradhan S, Demirgok B. Natural gas vehicles in heavy-duty transportation-A review. Energy Pol 2018;122:253–9. https://doi.org/10.1016/j.enpol.2018.07.052.
[11] Dimitriou P, Kumar M, Tsujimura T, Suzuki Y. Combustion and emission characteristics of a hydrogen-diesel dual-fuel engine. Int J Hydrogen Energy 2018;43:13605–17. https://doi.org/10.1016/j.ijhydene.2018.05.062.
[12] Di Iorio S, Magno A, Mancaruso E, Vaglieco BM. Analysis of the effects of diesel/methane dual fuel combustion on nitrogen oxides and particle formation through optical investigation in a real engine. Fuel Process Technol 2017;159:200–10. https://doi.org/10.1016/j.fuproc.2017.01.009.
[13] Di Iorio S, Magno A, Mancaruso E, Vaglieco BM. Characterization of particle number and mass size distributions from a small compression ignition engine operating in diesel/methane dual fuel mode. Fuel 2016;180:613–23. https://doi.org/10.1016/j.fuel.2016.04.108.
[14] Noll B, del Val S, Schmidt TS, Steffen B. Analyzing the competitiveness of low-carbon drive-technologies in road-freight: a total cost of ownership analysis in Europe. Appl Energy 2022;306:118079. https://doi.org/10.1016/j.apenergy.2021.118079.
[15] Korb B, Kuppa K, Nguyen HD, Dinkelacker F, Wachtmeister G. Experimental and numerical investigations of charge motion and combustion in lean-burn natural gas engines. Combust Flame 2020;212:309–22. https://doi.org/10.1016/j.combustflame.2019.11.005.
[16] Catapano F, Di Iorio S, Magno A, Sementa P, Vaglieco BM. A comprehensive analysis of the effect of ethanol, methane and methane-hydrogen blend on the combustion process in a PFI (port fuel injection) engine. Energy 2015;88:101–10. https://doi.org/10.1016/j.energy.2015.02.051.
[17] Subramanian B, Ismail S. Production and use of HHO gas in IC engines. Int J Hydrogen Energy 2018;43:7140–54. https://doi.org/10.1016/j.ijhydene.2018.02.120.
[18] Ramsay CJ, Dinesh KKJR, Fairney W, Vaughan N. A numerical study on the effects of constant volume combustion phase on performance and emissions characteristics of a diesel-hydrogen dual-fuel engine. Int J Hydrogen Energy 2020;45:32598–618. https://doi.org/10.1016/j.ijhydene.2020.09.021.
[19] Yu X, Li G, Du Y, Guo Z, Shang Z, He F, et al. A comparative study on effects of homogeneous or stratified hydrogen on combustion and emissions of a gasoline/hydrogen SI engine. Int J Hydrogen Energy 2019;44:25974–84. https://doi.org/10.1016/j.ijhydene.2019.08.029.
[20] Lee S, Kim G, Bae C. Effect of injection and ignition timing on a hydrogen-lean stratified charge combustion engine. Int J Engine Res 2022;23:816–29. https://doi.org/10.1177/14680874211034682.
[21] Miller AL, Cb S, Mc H, Gg A. Role of lubrication oil in particulate emissions from a hydrogenpowered internal combustion engine. Environ Sci Technol 2007;41(19):6828–35.
[22] Pirjola L, Karjalainen P, Heikkila J, Saari S, Tzamkiozis T. Effects of fresh lubricant oils on particle emissions emitted by a modern gasoline direct injection passenger car. Environ Sci Technol 2015;49:3644–52. https://doi.org/10.1021/es505109u.
[23] Singh AP, Pal A, Agarwal AK. Comparative particulate characteristics of hydrogen, CNG, HCNG, gasoline and diesel fueled engines. Fuel 2016;185:491–9. https://doi.org/10.1016/j.fuel.2016.08.018.
[24] Miller AL, Stipe CB, Habjan MC, Ahlstrand GG. Role of lubrication oil in particulate emissions from a hydrogen-powered internal combustion engine. Environ Sci Technol 2007;41:6828–35. https://doi.org/10.1021/es070999r.
[25] Singh AP, Pal A, Gupta NK, Agarwal AK. Particulate emissions from laser ignited and spark ignited hydrogen fueled engines. Int J Hydrogen Energy 2017;42:15956–65. https://doi.org/10.1016/j.ijhydene.2017.04.031.
[26] Thawko A, Yadav H, Eyal A, Shapiro M, Tartakovsky L. Particle emissions of direct injection internal combustion engine fed with a hydrogen-rich reformate. Int J Hydrogen Energy 2019;44:28342–56. https://doi.org/10.1016/j.ijhydene.2019.09.062.
[27] Agudelo-Castañeda D, Teixeira E, Schneider I, Lara SR, Silva LFO. Exposure to polycyclic aromatic hydrocarbons in atmospheric PM1.0 of urban environments: carcinogenic and mutagenic respiratory health risk by age groups. Environ Pollut 2017;224:158–70. https://doi.org/10.1016/j.envpol.2017.01.075.
[28] Ciarkowska K. Assessment of heavy metal pollution risks and enzyme activity of meadow soils in urban area under tourism load: a case study from Zakopane (Poland). Environ Sci Pollut Res 2018;25:13709–18.
[29] Silva LFO, Pinto D, Neckel A, Oliveira MLS. An analysis of vehicular exhaust derived nanoparticles and historical Belgium fortress building interfaces. Geosci Front 2020;11:2053–60. https://doi.org/10.1016/j.gsf.2020.07.003.
[30] Di Iorio S, Sementa P, Vaglieco BM, Catapano F. An experimental investigation on combustion and engine performance and emissions of a methane-gasoline dual-fuel optical engine. SAE Tech Pap 2014;1. https://doi.org/10.4271/2014-01-1329.
[31] Johnson T, Caldow R, Pöcher A, Mirme A, Kittelson D. A new electrical mobility particle sizer spectrometer for engine exhaust particle measurements. SAE Tech Pap 2004;2004. https://doi.org/10.4271/2004-01-1341.
[32] TSI. Updated inversion matrices for engine exhaust particle sizer TM (eeps TM) spectrometer model 3090-application

note EEPS-005 (A4). https://tsi.com/products/particle-sizers/fast-particle-sizer-spectrometers/engine-exhaust-particle-sizer-(eeps)-3090/. 2015.
[33] Apicella B, Mancaruso E, Russo C, Tregrossi A, Maddalena M, Ciajolo A, et al. E ff ect of after-treatment systems on particulate matter emissions in diesel engine exhaust. Exp Therm Fluid Sci 2020;116:110107. https://doi.org/10.1016/j.expthermflusci.2020.110107.
[34] Gargiulo V, Apicella B, Stanzione F, Tregrossi A, Millan M, Ciajolo A, et al. Structural characterization of large polycyclic aromatic hydrocarbons. Part 2: solvent-separated fractions of coal tar pitch and naphthalene-derived pitch. Energy Fuel 2016;30(4):2574–83. https://doi.org/10.1021/acs.energyfuels.5b02576.
[35] Russo C, Carpentieri A, Tregrossi A, Ciajolo A, Apicella B. Blue, green and yellow carbon dots derived from pyrogenic carbon: structure and fluorescence behaviour. Carbon N Y 2023;201:900–9. https://doi.org/10.1016/j.carbon.2022.09.062.
[36] Apicella B, Millan M, Herod A, Carpentieri A, Pucci P, Ciajolo A. Separation and measurement of flame-formed high molecular weight polycyclic aromatic hydrocarbons by size-exclusion chromatography and laser desorption/ionization time-of-flight mass spectrometry. Rapid Commun Mass Spectrom 2006;20(7):1104–8. https://doi.org/10.1002/rcm.2419.
[37] Berlman IB. Fluorescence spectra of aromatic molecules. New York and London: Academic P.; 1971.
[38] Apicella B, Ciajolo A, Tregrossi A. Fluorescence spectroscopy of complex aromatic mixtures. Anal Chem 2004;76:2138–43. https://doi.org/10.1021/ac034860k.
[39] Alfè M, Apicella B, Barbella R, Tregrossi A, Ciajolo A. Distribution of soot molecular weight/size along premixed flames as inferred by size exclusion chromatography. Energy Fuels 2007;21:136–40. https://doi.org/10.1021/ef060320p.
[40] D'Anna A, Ciajolo A, Alfè M, Apicella B, Tregrossi A. Effect of fuel/air ratio and aromaticity on the molecular weight distribution of soot in premixed n-heptane flames. Proc Combust Inst 2009;32 I:803–10. https://doi.org/10.1016/j.proci.2008.06.198.
[41] Krzyszczak A, Czech B. Occurrence and toxicity of polycyclic aromatic hydrocarbons derivatives in environmental matrices. Sci Total Environ 2021;788. https://doi.org/10.1016/j.scitotenv.2021.147738.
[42] Liu Y, Ding A, Sun Y, Xia X, Zhang D. Impacts of n-alkane concentration on soil bacterial community structure and alkane monooxygenase genes abundance during bioremediation processes. Front Environ Sci Eng 2018;12(5). https://doi.org/10.1007/s11783-018-1064-5.
[43] Russo C, Apicella B, Ciajolo A. Blue and green luminescent carbon nanodots from controllable fuel-rich flame reactors. Sci Rep 2019;9:1–8. https://doi.org/10.1038/s41598-019-50919-1.